Proceedings of the 2004 IEEE
International Conference on Robotics & Automation
New Orleans, LA • April 2004

The Design, Fabrication, and Characterization of Millimeter Scale Motors For Miniature Direct Drive Robots

J. A. Palmer, J. F. Mulling, B. Dessent, E. Grant, J. W. Eischen, A. Gruverman, A. I. Kingon, P. D. Franzon
North Carolina State University
Center for Robotics and Intelligent Machines
Department of Electrical and Computer Engineering
Raleigh, NC, U.S.A.

Abstract – **This paper reports on research into miniature, direct drive, high force/torque motors to support insect-sized mobile robotic platforms. The primary focus is on scalable motors based on piezoelectric transducers. The contributions of this work include: (1.) the design, analysis, and characterization of a miniature mode conversion rotary ultrasonic motor based on a piezoelectric stack transducer; this produced a static torque density of 0.37 Nm/kg, (2.) a millimeter scale linear piezomotor, constructed with a parallel arrangement of annular stressed unimorph piezoelectric transducers and passive latches, exhibited 0.23 N of blocked force, and (3.) Simulation data is presented that compares these motor concepts to commercial systems in the context of scalability. Results suggest that smaller versions of the rotary ultrasonic motor would possess a static torque density seven times that of a commercial 3-mm electromagnetic system. This technology shows promise for driving the platform.**

Index Terms – Piezoelectric,scale,ultrasonic motor.

I. Introduction

A recent area of interest in the growing trend toward miniaturization of engineering systems is the development of "swarms" of millimeter scale distributed robots with sensory, energy, and power actuation systems that mimic insect architecture and locomotion. To master the physical principle, the biology of several species of jumping insects and amphibians was reviewed, such as frogs and locusts (Chapman and Joern) [1]. These animals share a common system whereby muscles stretch or compress a flexible protein to store elastic energy in a manner similar to a catapult [1]. A skeletal element serves as a latch which, when triggered, instantly releases the energy to a folding leg linkage that launches the body upward [1]. A macro scale prototype of a robotic jumping platform shown in Fig. 1 mimics the components of such biological systems. In this design, elastic energy is stored in sets of parallel coil springs. In the linear configuration, the rod is driven by a linear motor with an integral passive latch acting as the trigger. A modified version used a rotary motor connected to a cam-follower mechanism, with the geometry of the cam governing the triggering action. Since the height of the jump is dependent on the mass of the platform, it was necessary to design the drive mechanism with motors less than one inch in length and diameter

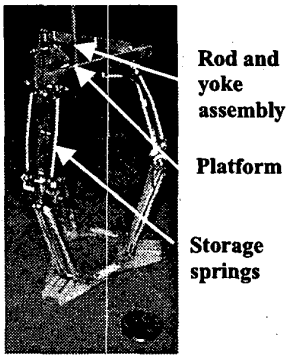

Figure 1. Robotic jumping platform.

to directly drive the folding leg linkage without mechanical force/torque amplification (Fig. 1). The following segment provides justification for selecting piezoelectric transducer technology to create a rotary ultrasonic motor, and a linear non-ultrasonic piezomotor, based on simple, scalable designs.

II. Rotary Ultrasonic Motor

Conventional electromagnetic motors suffer a significant decrease in static torque capability at the millimeter scale (Khatib, Craig, and Lozano-Perez) [2]. As motor volume decreases, output power is dominated by high angular velocity (recall power is the product of torque and angular velocity) (Mulling) [3]. This research addresses the "motor gap" in direct drive micro robotics applications by developing a miniature rotary ultrasonic motor. Rotary ultrasonic motors (USM's) convert one or more harmonic signals to a standing or traveling acoustic wave at tens of kilohertz by means of one or more piezoelectric transducers assembled in a resonator (Ragulskis, Bansevicius, Barauskas, and Kulvietis) [4], (Uchino) [5]. The vibration is mechanically coupled to a rotor to generate useful rotary motion and torque. Rotary USM's deliver high torque at low rotational velocities, whereas DC servomotors require a reduction gearbox, which adds weight, cost, and control complexity (Uchino) [5]. Additionally, many USM designs

0-7803-8232-3/04/$17.00 ©2004 IEEE

consist of a few simple, fixed parts and no copper windings, making them favorable for miniaturization [5]. USM's suffer significant efficiency losses due to frictional contact between rotor and stator and powering them is difficult, as they require a high voltage dynamic circuit operating at ultrasonic frequency. Noting these drawbacks, the single transducer "mode conversion" USM inspired by the Kumada design was ultimately selected (Kumada) [6], [5]. It has been successfully implemented by Yao, Koc, and Uchino (Yao, Koc, and Uchino) [7], and exhibits greater static torque density than USM's of comparable mass (Glenn and Hagood) [8]. Its simple, "tonpilz" resonator is well understood (Stansfield) [9]. The Kumada design is reversible with frequency in contrast to other USM's that alter direction more reliably by shifting the relative phase of multiple drive signals [7, 8].

Fig. 2 depicts the prototype USM. The tonpilz resonator consists of an annular piezoceramic lead zirconate titanate (PZT) layered stack transducer that undergoes an axial strain when an electric field is applied [5]. The transducer is attached to a set of steel masses using epoxy. The tail mass is designed with greater volume and inertia than the head mass in order to direct the kinetic energy of vibration forward toward the rotor [5]. A bolt threaded through the center of the head and tail masses maintains the necessary compressive stress in the transducer. A longitudinal-torsional (L/T) coupler is mounted to the head mass at its outer perimeter, completing the stator assembly. The beam or spine on the L/T coupler is offset from the vertical plane of symmetry by an angle of 154 degrees (note the supplementary angle of 26 degrees is shown for clarity) [6]. Fig. 3 illustrates how the L/T coupler deforms to convert the longitudinal vibration of the stator to an *elliptical*displacement locus at the outlying edges of the beam where embedded spherical contacts (not shown) engage the face of the rotor. This unique L/T coupler mode shape occurs at the resonant frequency of the stator assembly, which is referred to here as the *primary operating frequency*. In powered demonstrations, USM ran consistently at the primary operating frequency of 43 kHz.

At the primary operating frequency, during the *drive stroke*, the stator expands upward (longitudinally), while the tip of the L/T coupler deflects laterally (tangentially). The reverse motion occurs during the *return stroke*, where the stator works against the rotor. Assuming the rotor is rigid, and the pre-load spring maintains

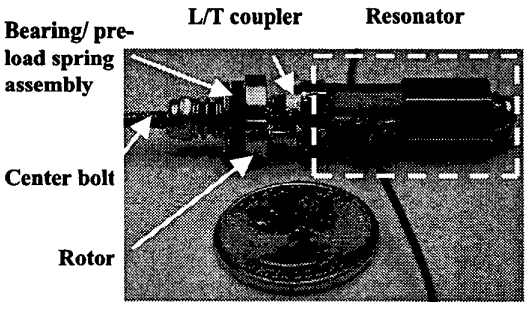

Figure 2. Miniature mode conversion USM prototype.

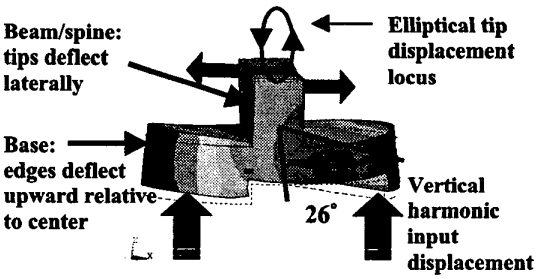

Figure 3. L/T coupler deformed view.

continuous rotor/stator contact, the harmonic motion generates a dynamic or time-varying pre-load force denoted by n_θ (Ueha and Tomikawa) [10]. It is written as follows:

$$n_\theta = N_0(1+\sin(\omega t+\phi)) \tag{1}$$

where N_0 is the static pre-load force, ω is the drive signal frequency in radians per second, and ϕ is the phase difference in radians relative to the input signal. Assuming there is a non-zero phase difference φ between the longitudinal and tangential components of the stator displacement, the magnitude of the dynamic pre-load force is larger on the drive stroke than on the return [10]. Hence there is a resultant frictional torque available to continuously drive the rotor. Mathematically, this hypothesis implies that the instantaneous torque changes its sense from positive to negative whenever the difference between the rotor (R) and stator (S) velocities changes sign during the drive signal period. With the operating principles established, the equation of motion for the mode conversion USM is expressed as the following [5, 10]:

$$J_0\ddot{\theta}_R + c_t\dot{\theta}_R = \mathrm{sgn}\,|\dot{\theta}_R - \dot{\theta}_S|\,\mu_k n_\theta d_{eff} - \tau_{load} \tag{2}$$

where J_0 is the polar mass moment of inertia of the rotor and thrust bearing (Rao) [11], μ_k is the coefficient of kinetic friction, d_{eff} is the distance between the stator contact points, and c_t is the coefficient of coulomb damping between the rotor and hub (assumed to be zero in this program) (Wallaschek) [12]. The rotational velocity of the stator involves differentiating the measured tangential displacement as follows:

$$\dot{\theta}_S = \frac{2A_2\omega}{d_{eff}}\cos(\omega t + \phi + \varphi) \tag{3}$$

where A_2 is the measured peak-to-peak tangential amplitude, and φ represents the phase difference between the longitudinal and tangential displacements. Static (stalled rotor) torque is calculated as follows: a static load torque τ_{load} is added to the right side of (2) and, using a numerical integration technique, the equation is solved repeatedly for a series of load values to create a theoretical rotor velocity versus load plot. The static torque corresponds to the load for which the rotor velocity is reduced to zero. Static torque density follows from the ratio of the static torque to the mass of the prototype.

III. LINEAR PIEZOMOTOR

A non-ultrasonic linear motor constructed from piezoelectric transducers is referred to as the linear piezomotor [5]. The linear piezomotor architecture consists of a set of clamps, coupled with the transducer acting as an extender. The clamps alternately lock the device, thereby allowing the extender to force one segment to move relative to the other. The result is an inchworm motion along a rod or fixed guide. Many linear piezomotor designs feature actively controlled clamps assisted by mechanisms that amplify the transducer strains Xu and King [13]. To remove the need for external amplification, other classes of piezoelectric transducers, stressed unimorphs, have been developed (Hyder, Horner, and Clark), [14].

A device designated a thin layer composite unimorph ferroelectric driver and sensor (THUNDER™) is created by bonding a piezoceramic and aluminum laminate to a spring steel substrate using a polyimide adhesive (Wise) [15]. The adhesive curing process introduces residual stresses into the composite structure. The complete transducer has a curved substrate that mechanically amplifies piezoelectric deflection. Accordingly, THUNDER™ transducers exhibit a flexural displacement many times that of stack transducers by virtue of their construction. Fig. 4 shows the annular THUNDER™ transducer. A THUNDER™ is a *compliant* structure. When a voltage is applied, bi-axial deformation occurs in the piezoceramic layer that reduces the radius of curvature of the substrate. When voltage is removed, work is performed as the compliant substrate returns the transducer to its equilibrium position. The amount of work depends upon the stiffness of the substrate and the end conditions of its mounting (Mulling, Usher, Dessent, Palmer, Franzon, Grant, and Kingon) [16]. An actuator system may be constructed by arranging THUNDERS in parallel. This arrangement increases the system stiffness, and impacts the amount of work that can be achieved.

The Milliworm miniature linear piezomotor was created from a parallel assembly 0.525-inch diameter annular THUNDER™ transducers. As an alternative to clamps, the design features latches that are passive in operation because they require no direct control. The latches are "mechanical diodes," permitting motion of the linear piezomotor in one direction only. The style of the latch used was patented by inventors such as Goul [17], and has been commercially available for decades. Fig. 5 depicts the Milliworm prototype. The housing and base plate are joined to the latch at the rear, while the transducer assembly connects to a latch

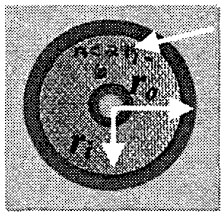

Figure 4. Annular THUNDER™.

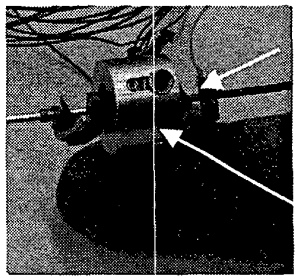

Figure 5. Milliworm linear piezomotor.

at the front. Milliworm is approximately 1 inch in length, and one half inch in diameter, weighing 10 grams. When powered by a 480-volt square wave at 50 Hz, the device generates inchworm motion along the rod.

The blocked output force of the Milliworm's transducer module can be classified in two ways: (1.) the free mass type, F_1, denotes a load level at which all flexural displacement of the module ceases, and, more importantly, (2.) the actuator type blocked force F_2 (a qualitative performance measure), causes static deflection equal to the powered flexural displacement with zero applied load, δ_0 (Palmer, Dessent, Mulling, Usher, Grant, Eischen, Kingon, and Franzon) [18]. Consequently, a load of this magnitude tends to reduce the elastic rebound of the module to approximately zero with no net forward motion of the piezomotor. This quantity is the product of δ_0 and the zero-potential equivalent stiffness, $K_{eq}(0)$:

$$F_2 = \delta_0 K_{eq}(0). \tag{4}$$

Equivalent dynamic systems theory prescribes that the effective actuator stiffness, K_{eq}, is the sum of the stiffnesses of the individual THUNDERS working in parallel [11]. This relationship is expressed as follows:

$$K_{eq}(V) = \sum_{i=1}^{n} k_i(V). \tag{5}$$

Stiffness k_i in the transducers is a function of the applied voltage, V. This notation reflects the tendency for stiffness to increase with tensile stress in the substrate as it flexes during actuation (Gere and Timoshenko) [19]. The following expression predicts the zero-load flexural displacement of the annular THUNDER™ at a radial position $r = r_h$, corresponding to the edge of the hole (see Fig. 5) when voltage is applied:

$$\delta_0 = C_1^* \frac{r_h^2}{4} + C_2^* \ln\left(\frac{r_h}{r_o}\right) + C_3^* \qquad (0 < r_h \le r_i) \tag{6}$$

where the C^* coefficients result from enforcing boundary conditions at the perimeter of the device ($r = r_o$), and at the substrate/composite material interface ($r = r_i$, see Fig. 5). The

boundary conditions include an expression for the piezoelectric moment M_p, which is a function of the voltage and the piezoelectric strain coefficient d_{31} that relates the strain due to lattice expansion in the vertical (z) direction (and corresponding radial constrictive strain) per unit of electric field applied to the piezoceramic (Coorpender, Finkel, Kyzar, Sims, Smirnova, Tawhid, Bouton, and Smith) [20]. Details of the piezoelectric moment formula are provided by Coorpender et al. [20]. Equation 6 assumes the annular THUNDER™ (with homogeneous material properties) is simply supported at the outer perimeter, and subjected to a uniform load q (equal to zero in this case) distributed over the upper surface area. Furthermore, the total thickness of the device must be small relative to its outer radius, and deflections are assumed to be less than one-half the total device thickness (Timoshenko and Woinowsky-Krieger) [21]. This configuration is representative of the device constraints in the Milliworm. Experimental data yields good agreement with (6) for transducers 0.525 to 0.875 inches in outer diameter.

IV. Results

The USM torque test procedure involved applying a load to the rotor, starting the prototype from rest, and measuring the corresponding steady state velocity using a non-contact laser gage. A battery-driven dynamic circuit provided power to the transducer. The rotor load was varied by mounting a series of weights on a brake pressed against a drive shaft coupled to the rotor of the prototype. The static torque was extrapolated from the linear plot of rotor velocity versus brake force. Modifying the prototype to accept a L/T coupler with a beam section 2.5 times longer than the standard Kumada design amplified the longitudinal displacement amplitude of the stator (and hence the dynamic preload amplitude) at the primary operating frequency. This led to the greatest measured static torque of 11.3 mNm in the 30.5-gram prototype, with a corresponding static torque density of 0.37 Nm/kg.

Dimensional analysis was applied to parameters associated with the mode conversion USM. Based on the results, conclusions are drawn regarding the scalability of the system. The simulation calculated the static torques and steady state rotor velocities of a set of geometrically similar mode conversion USM's (Baker) [22]. In constructing the simulation, the following USM dimensions were scaled linearly by an arbitrary factor of three quarters: radial and axial dimensions, including the distance between the L/T coupler ball bearing contacts, the outer and inner rotor radii, and the rotor, head mass, and tail mass thickness. Considering the axial displacement of a simple, single-layer, piezoelectric transducer is related to its length by the piezoelectric strain coefficient, the axial and tangential displacement of the USM stator was also scaled linearly by the same factor [5]. The magnitude of the static pre-load was scaled by this factor to reflect the change in axial displacement amplitude. Reducing the size (and the mass) of the resonator causes the primary operating frequency to increase [11]. To simulate this effect, a simple two-degree-of-freedom harmonic resonator model was utilized to estimate the primary operating frequency given the scaled dimensions of the head and tail masses [9]. A new equivalent stiffness of the transducer was calculated to improve the accuracy of the equation relative to the measured primary operating frequency of the prototype. Defining scale factor s_r as the ratio of the contact radii of two geometrically similar prototypes, the dimensional analysis results show that the static torque varies as s_r^2, and steady state rotor velocity as $s_r^{-1.5}$. Thus, if the radius of the USM is halved, the static torque decreases by one quarter. Furthermore, miniaturization will cause the steady state rotor velocity to increase by a power of three halves. Dimensional analysis results support the conclusion that smaller versions of the prototype mode conversion USM exhibit greater static torque density and lower steady state speed than electromagnetic (EM) motors of similar size. Table I lists performance data associated with a simulated mode conversion USM with a 1.7-mm contact radius, and a 3-mm diameter Smoovy® EM motor [3]. The

TABLE I
Simulated Micromotor Performance [3]

Parameter	Simulated Mode Conversion USM (1.7-mm contact radius)	3-mm diameter Smoovy® EM motor
Mass (g)	3 (estimated)	0.33
Steady state rotor velocity (rpm)	3,691	72,000
Static torque (mNm)	2.3	0.035
Static torque density (Nm/kg)	0.77	0.11
Power density (W/kg)	81 (peak) @ 1978 rpm	1,340

Smoovy® generates greater power due to its higher steady state speed. Although the Smoovy® has a significant advantage in mass, the static torque density remains seven times smaller than the USM.

The Milliworm prototype was characterized to measure its performance relative to predictions, and to identify failure modes. Using a LVDT test apparatus, a blocked output force of 0.23 N was measured with a corresponding power density of 9.4 mW/kg. Blocked force performance was affected by limitations in the design of the module and latches, and the straightness of the rod. These factors work in concert to reduce the stiffness of the piezomotor, reduce its step displacement under load, and increase the level of frictional resistance. A blocked force characterization of the 0.525-inch transducers revealed that gaps and compliant parts in the coupling and "C" ring assemblies contribute to settling in the extender module, which dramatically reduces its stiffness. Furthermore, displacement losses caused by back slip the passive latches reduce the displacement output of the extender module in a

given cycle. The amount of displacement loss depends on the load level. These observations suggest that the amount of powered deflection (which partly determines the amount of elastic rebound) in the THUNDER™ transducers per drive cycle is an important factor in the consistent operation and, indirectly, the blocked force performance in smaller versions of the Milliworm piezomotor.

To quantify the relationship between powered deflection and size, an expression that relates δ_0 exclusively in terms of the outer radius r_o was derived. First, the hole radius and the outer radius of the piezoceramic layer were related to the outer radius of the transducer by constant fractions (see Fig. 4). Specifically, r_h is $0.142r_o$, and r_i is $0.865r_o$. Assigning values to the material properties and making the aforementioned substitutions in the expressions for coefficients C^* (omitted) reveal that $C_1^* = a_0$, $C_2^* = a_1 r_o^2$, and $C_3^* = a_2 r_o^2$, where a_0, a_1, and a_2 are constants. Substituting these expressions into (6) results in:

$$\delta(0.142r_o) = \left(\frac{a_0(0.142)^2}{4} + \ln(0.142)a_1 + a_2 \right) r_o^2 \quad (7)$$

Equation 7 suggests that the deflection of the annular THUNDER™ is directly proportional to the square of the outer radius. This finding is consistent with experimental deflection data, in addition to documented results for the maximum deflection of a simply supported homogeneous circular plate under a central point load [11, 21]. As a consequence of the scale relationship, the no-load powered deflection of the annular THUNDER™ is reduced rapidly with outer radius to a practical limit of five to ten microns for transducers less than one-half inch in diameter. It follows that stack-type transducers become a more attractive alternative to annular THUNDERS in smaller versions of the Milliworm design.

V. Conclusions And Future Work

Two miniature piezoelectric motors have been prototyped and characterized for use with a biomimetic robot. Both systems are novel in the context of their size, simplicity, and scalability. The miniature mode conversion rotary USM exhibited greater power density than the linear piezomotor, and is predicted to have greater scalability. It follows that the rotary USM is considered more suitable for this application. On the micro scale (defined by a contact radius less than 1 mm), the USM will not be effective as a direct drive motor, as the unloaded steady state rotor velocity is expected to rise above 4,000 rpm. Dynamic simulation data indicates that a geometrically similar micro-scale version of the mode conversion USM prototype would possess greater static torque density and lower steady state rotor velocity than one of the smallest commercial EM motors currently available: the 3-mm diameter Smoovy®. This result supports the literature [5, 10] in the claim that with respect to torque and speed, rotary USM's are more effective than EM motors in miniature direct drive robotics applications.

Characterization trials with the Milliworm linear piezomotor illustrated the difficulties associated with producing piezomotor actuation based on micron-sized transducer displacements due to the loss of displacement with diameter, and the difficulty in coupling it. It is anticipated that the cost associated with precision engineering of the module will climb as annular transducer displacements decrease with the square of the outer radius.

References

[1] Chapman, R.F. and Joern, A., *Biology of Grasshoppers*, New York: John Wiley and Sons, 1990.

[2] Khatib, O., Craig, J.J. and Lozano-Perez, T., *The Robotics Review 2*, Cambridge, Massachusetts: The MIT Press, 1992.

[3] Mulling, J.F., "Compiled performance metrics for linear and rotary actuators and motors," North Carolina State University Center for Robotics and Intelligent Machines, Technical Report NCSU-CRIM-TR-2002-0202, 2002.

[4] Ragulskis, K., Bansevicius, R., Barauskas, R., and Kulvietis, G., *Vibromotors for Precision Microrobots*, New York: Hemisphere Publishing Corporation, 1988.

[5] Uchino, K., *Piezoelectric Actuators and Ultrasonic Motors*, Boston : Kluwer Academic Publishers, 1997.

[6] Kumada, A., "Ultrasonic motor using bending, longitudinal and torsional vibrations." United States Patent 4,642,509, 1987.

[7] Yao, K., Koc, B., and Uchino, K., "Longitudinal-bending mode micromotor using multilayer piezoelectric actuator," *IEEE Transactions on Ultrasonics, Ferroelectrics and Frequency Control*, vol. 48, num. 4, pp. 1066 –1071, 2001.

[8] Glenn, T.S., and Hagood, N.W., "Development of a two-sided piezoelectric rotary ultrasonic motor for high torque," *SPIE Smart Structures and Integrated Systems*, vol. 3041, pp. 326-338, 1997.

[9] Stansfield, D., *Underwater Electroacoustic Transducers: A Handbook for Users and Designers*, Bath, UK: Bath University Press, 1991.

[10] Ueha, S. and Tomikawa, Y., *Ultrasonic Motors: Theory and Applications*, New York: Oxford University Press, 1993.

[11] Rao, S. S., *Mechanical Vibrations*, 3rd ed., Reading, Massachusetts: Addison-Wesley Publishing Company, 1995.

[12] Wallaschek, J., "Contact mechanics of piezoelectric ultrasonic motors," *Smart Materials and Structures*, vol. 7, pp. 369-381, 1998.

[13] Xu, W., and King, T.G., "Piezomotors using flexure hinged displacement amplifiers," *IEE Colloquium on Innovative Actuators for Mechatronic Systems*, vol. 11, pp. 1-5, 1995.

[14] Hyder, C., Horner, G., and Clark, W., "Linear traveling wave motor," *SPIE Conference on Industrial and Commercial Applications of Smart Structures Technologies*, vol. 3674, pp. 205-211, 1999.

[15] Wise, S. A., "Displacement properties of RAINBOW and THUNDER piezoelectric actuators," *Sensors and Actuators A: Physical*, vol. A 69, pp. 33-38, 1998.

[16] Mulling, J., Usher, T., Dessent, B., Palmer, J., Franzon, P., Grant, E., and Kingon, A., "High displacement piezoelectric actuators: characterization at high load with controlled end conditions," *Sensors and Actuators A: Physical*, vol. 94, pp. 19-24, 2001.

[17] Goul, A.S., "Fast clamp," United States Patent Number 4,874,155, 1989.

[18] Palmer, J. A., Dessent, B., Mulling, J. F., Usher, T., Grant, E., Eischen, J. W., Kingon, A. I., and Franzon, P. D., "The design and characterization of a novel piezoelectric transducer-based linear motor," (unpublished).

[19] Gere, J.M., and Timoshenko, S.P., *Mechanics of Materials*, 4th ed., New York: PWS Publishing, 1997.

[20] Coorpender, S., Finkel, D., Kyzar, J., Sims, R., Smirnova, A., Tawhid, M., Bouton, C., and Smith, R.C., "Modeling and optimization issues concerning a circular piezoelectric actuator design," *Adaptive Structures and Materials Systems 1999*, pp. 199-204, 1999.

[21] Timoshenko, S., and Woinowsky-Krieger, S., *Theory of Plates and Shells*, 2nd ed., New York: McGraw-Hill, Inc., 1959.

[22] Baker, W.E., Westine, P.S. and Dodge, F.T., *Similarity Methods in Engineering Dynamics*, New York: Elsevier, 1991.

ACKNOWLEDGEMENTS

The authors are grateful to DARPA for support of this program under contract number N3998-98-C3536.

CORRESPONDENCE INFORMATION

japalme@sandia.gov, bedessen@nando.net, egrant@eos.ncsu.edu, eischen@eos.ncsu.edu, alexei_gruverman@ncsu.edu, angus_kingon@ncsu.edu, paulf@ncsu.edu